Synthesis of amorphous KAlSi$_3$O$_8$ for cesium radionuclide immobilization into solid matrices using spark plasma sintering technique

S.B. Yarusova [a,b], O.O. Shichalin [a,c], A.A. Belov [a,c], S.A. Azon [c], I. Yu Buravlev [a,c], A.V. Golub [a], V. Yu Mayorov [a], A.V. Gerasimenko [a], E.K. Papynov [a,c,*], A.I. Ivanets [d], A.A. Buravleva [c], E. B. Merkulov [a], V.A. Nepomnyushchaya [c], O.V. Kapustina [c], P.S. Gordienko [a]

[a] *Institute of Chemistry, Far Eastern Branch of Russian Academy of Sciences, 159, Prosp. 100-letiya Vladivostoka, Vladivostok, 690022, Russia*
[b] *Vladivostok State University of Economics and Service, Gogolya st., 41 Vladivostok, 690014, Russia*
[c] *Far Eastern Federal University, 10 Ajax Bay, Russky Island, 690922, Vladivostok, Russia*
[d] *Institute of General and Inorganic Chemistry of National Academy of Sciences of Belarus, Surganova st. 9/1, Minsk, 220072, Belarus*

ARTICLE INFO

ABSTRACT

An effective sorption material for cesium radionuclides immobilization in highly safe and reliable solid-state matrices was proposed. Prepared aluminosilicate (KAlSi$_3$O$_8$) adsorbent had amorphous mesoporous structure and Cs$^+$ ions sorption capacity of ~3.7 mmol/g. The physical-chemical characteristics of (Cs, K)AlSi$_3$O$_8$ sample saturated with Cs$^+$ ions were studied using XRD, FT-IR, SEM-EDX, and DTA-TG methods. Firstly, solid-state aluminosilicate matrices were obtained using spark plasma sintering (SPS) technology with high values of relative density (up to 99.9%), compressive strength (31.3–79.2 MPa), and Vickers microhardness (0.9–5.3 GPa). The sample obtained at 1000 °C had a low value of Cs$^+$ leaching from matrices (R$_{Cs}$ within the range of 10^{-7} g cm^{-2}·day^{-1}) and cesium diffusion coefficient (D$_e$ 9.07×10^{-14} cm^2/s). It was shown that prepared aluminosilicate cesium matrices comply with regulatory requirements of GOST R 50926-96 and ANSI/ANS 16.1.

1. Introduction

Novel inorganic materials used for the sorption and immobilization of hazardous radionuclides are extremely important for the technological aspects of radioactive waste management. Solid-state matrices provide the required set of such operational characteristics as chemical activity/inertia, radiation resistance, hydrolytic resistance, mechanical strength, etc. These materials are used as selective sorbents for the processing of liquid radioactive wastes [1–3], as well as preserving matrices for the immobilization of extracted radionuclides for their subsequent reliable disposal [4] or the production of high-class radioisotope products [5]. Therefore, these materials provide a new high level of safety for the nuclear industry, including by ensuring the large-scale global task of implementing a closed nuclear fuel cycle.

Aluminosilicates of natural and synthetic origin, as well as their modified forms, are considered as a promising class of compounds for the selective sorption of long-lived hazardous ^{137}Cs and ^{90}Sr radionuclides. Various aluminosilicate minerals (montmorillonite (Na,

Ca)$_{0.33}$(Al,Mg)$_2$(Si$_4$O$_{10}$)(OH)$_2$·nH$_2$O [6], illit (K$_{0.75}$(H$_3$O)$_{0.25}$)Al$_2$(Si$_3$Al) O$_{10}$((H$_2$O)$_{0.75}$(OH)$_{0.25}$)$_2$ [7], kaolin Al$_2$O$_3$·2SiO$_2$·2H$_2$O and bentonite (Al$_2$[Si$_4$O$_{10}$](OH)$_2$·nH$_2$O) [8], chabazite (Ca,Na$_2$) [Al$_2$Si$_4$O$_{12}$]•6H$_2$O [9], vermiculite (Mg^{+2}, Fe^{+2}, Fe^{+3})$_3$ [(Al,Si)$_4$O$_{10}$]·(OH)$_2$·4H$_2$O [10], feldspars K[AlSi$_3$O$_8$], Na[AlSi$_3$O$_8$], Ca[Al$_2$Si$_2$O$_8$] [11], zeolites X$_{x/n}$ [(AlO$_2$)$_x$ (SiO$_2$)$_y$] [12]), as well as their synthetic analogs were widely described. These materials were obtained by well-known inorganic synthesis methods: hydrothermal, sol-gel, precipitation and co-precipitation, microwave [13–16]. Meanwhile, they did not receive wide practical application due to the following disadvantages: (i) low efficiency of radionuclides sorption by natural minerals, (ii) the complexity of industrial scaling of obtaining synthetic aluminosilicates analogs.

A capable of forming dense glass-like (amorphous) or ceramic (crystalline) forms of materials with chemically bound radionuclides with certain technological processing are the special advantage of aluminosilicate sorbents. This is a certain type of cured radioactive waste in the form of radionuclide-immobilized matrices. In the reviews

of Orlova and Ojovan [4,17], various types of frame aluminosilicates of natural origin were considered: zeolites $X_{x/n}$ [$(AlO_2)_x$ $(SiO_2)_y$], pollucite $(Ca,Na)_2Al_2Si_4O_{12}$ $2H_2O$, nepheline $NaAlSiO_4$, sodalite $(Na, K)_6[Al_6Si_6O_{24}]·2NaCl$, cancrinite $(Na,Ca,K)_6[Al_6Si_6O_{24}]((Na,Ca, K)_2CO_3)_{1.6}·2.1H_2O$, etc. Such materials demonstrated relatively high prospects for the wide range radionuclides immobilization, including ^{137}Cs and ^{90}Sr. A distinctive feature of these materials is that the methods of inorganic synthesis provide the production of their synthetic analogs, the characteristics, and properties of which could be enhanced in comparison with natural forms.

In the work of Omerasevic et al. [18], a dense (99.4%), mechanically strong (50.21 MPa), and Cs^+ leaching resistance (10^{-4} $g/cm^2·day$) pollucite ($CsAlSi_2O_{12}$) was obtained by hot pressing from Ca-LTA ion-exchange zeolite. Vereshchagina et al. [19] synthesized the glass-ceramic matrices based on pollucite-nepheline and strontium feldspar from coal ash under hydrothermal conditions, which are promising for binding ^{137}Cs and ^{90}Sr. The liquid-phase sintering was applied by Luo et al. [20] for the production of ceramics based on strontium anorthite ($SrAl_2Si_2O_8$) of a monoclinic structure for the immobilization of strontium with a density of up to 3.02 g/m^3, bending strength of up to 60 MPa, and a volume porosity of 0.52 vol%. Chen et al. [21] synthesized the metakaolin/Na-pollucite composite by cold pressing followed by sintering in air, which was characterized by a mechanical strength of up to 48 MPa with high hydrolytic resistance to cesium leaching. A similar approach of direct sintering without pressure was used by Gardner et al. [22] for the preparation of ceramic matrices based on ultra-stable H–Y zeolite ($Na_{12}[(AlSiO_4)_{12}]$) for the cesium and strontium radionuclides immobilization. The main disadvantages of proposed methods are high duration of heat treatment to obtain ceramic matrices and low reproducibility of the physical-chemical properties of the resulting ceramic matrices.

Enhanced performance characteristics of ceramic and glass-ceramic matrices based on pollucite ($CsAlSi_2O_6$) for the immobilization of cesium, as well as mineral-like matrices based on strontium feldspar ($SrAl_2Si_2O_8$) for the immobilization of strontium, were achieved using an unconventional spark plasma sintering (SPS) technology and its reaction modification (R–SPS) in the works of Papynov E.K. et al. [23–25]. These matrices were characterized by high relative density (up to 99.8%), mechanical compressive strength (up to ~ 700 MPa), low leaching rate (do not exceed 10^{-6} $g/cm^2·day$), thermal stability during oxidative heating (up to 1000 °C) with a Cs^+ content of up to 24.5 wt% and Sr^{2+} up to 32 wt%. The obtained solid-state matrices exceeded the requirements of regulatory standards and the characteristics of analog materials. The originality of the proposed methods was that these matrices were obtained based on both natural and synthetic raw materials, with more attractive technological conditions (low temperature, short cycle time) compared to traditional sintering methods. Moreover, a method for manufacturing glass-ceramic matrices with cesium in the product of an ionizing radiation source using SPS technology characterized by the process efficiency was developed [26]. Despite this, achieving even higher characteristics of these materials using even cheaper raw materials remains an urgent research task.

Gordienko P.S. et al. [27] showed that the synthetic nanostructured potassium aluminosilicate $KAlSi_3O_8·1.5H_2O$ of the amorphous composition obtained in a multicomponent aqueous system containing an alkali metal silicate with a given SiO_2/K_2O ratio was characterized by a high sorption capacity towards Cs^+ ions, including under conditions of different salt background. This value reached the maximum, theoretically possible cation exchange centers in the range of 3.7 mmol/g. It was obvious that this system, obtained in a simple and fast way, represented a prospect as a sorption material for ^{137}Cs removal from aqueous media, and could be used as an inorganic basis for obtaining solid-state matrices for reliable radionuclide immobilization, and conditioning the spent sorbent. In this regard, this work aimed to syntheses the solid-state matrices for cesium ions immobilization based on amorphous $KAlSi_3O_8$ using SPS technology with low Cs^+ leaching and high thermal

stability.

2. Experimental

The synthesis of amorphous potassium aluminosilicate powder ($KAlSi_3O_8$) and samples of solid-state matrices and their complex study was implemented according to the scheme (Fig. 1):

2.1. Chemicals

Aluminum sulfate $Al_2SO_4·18H_2O$ (99.9%, Sigma-Aldrich), potassium hydroxide KOH (Sigma-Aldrich), silicic acid $SiO_2·nH_2O$ (99.99%, Sigma-Aldrich) reagents without additional purification were used. The model solution of cesium chloride with a concentration of Cs^+ 25.2 mmol/L (3350 mg/L) was prepared from the CsCl (99.98, Sigma-Aldrich) reagent.

2.2. Synthesis of $KAlSi_3O_8$ powder

To obtain potassium aluminosilicate with a given Si/Al ratio ($KAlSi_xO_y·nH_2O$, where x = 3, y = 2(x+1)), the system components were taken in a stoichiometric ratio based on the calculation of obtaining anhydrous $KAlSi_3O_8$ aluminosilicate. A suspension of silicic acid was added to a KOH solution at 85 °C, kept under constant stirring until it was completely dissolved. Then, a solution of $Al_2(SO_4)_3$ was added to the resulting solution with continuous stirring. The resulting precipitate was separated by filtration using a water jet pump, washed with distilled water, and dried at 95 °C.

2.3. Sorption characteristics of $KAlSi_3O_8$ powder

Preliminary, the obtained precipitate was dried to a constant weight at a temperature of 105 °C. Further, the adsorbent was saturated under static conditions with a CsCl solution (Cs^+ 25.2 mmol/L) at a ratio of solid to liquid phases S:L equal to 1:40 and a temperature of 20 °C for 3 h with stirring at 150 rpm on an RT 15 power magnetic stirrer (IKA WERKE, Germany). Then the adsorbent was separated from the solution by filtering through the filter paper "White Ribbon Filter" (pore size 5–8 μm, ash content 0.26–0.31 mg) using a water jet pump. The concentration of Cs^+ and K^+ ions in the solutions was determined by atomic absorption spectrometry on a Solaar M6 spectrometer along the analytical lines of 852.1 and 766.5 nm, respectively. The precipitate was thoroughly washed with hot distilled water until the negative reaction towards Cl-ions.

2.4. Spark plasma sintering of (K, Cs)$AlSi_3O_8$ solid matrices

(K, Cs)$AlSi_3O_8$ powder was consolidated by SPS technique into solid matrices using LABOX-625 (Japan) instrument. The starting powder was put into cylindrical graphite die (outer diameter of 30 mm, internal diameter of 15.3 mm, height of 30 mm), pre-pressed (20.7 MPa), further the green body was transferred into a vacuum chamber (6 Pa) and
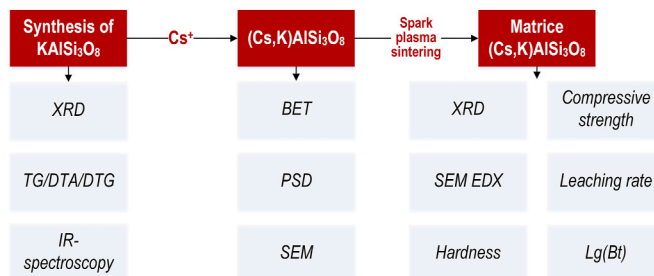
Fig. 1. General scheme of synthesis and research of adsorbent and ceramic matrices saturated with cesium ions.

sintered. Heating was conducted by the pulse current in the On/Off regime with the periodicity of the pulse/pause of 12/2 (39.6/6.6 ms). Synthesis temperature was 800, 900, 1000 °C, heating rate – 100 °C/min holding time at maximum temperature and cooling time were 5 and 30 min, respectively. The uniaxial pressure load during sintering was maintained constant at 24.5 MPa. The obtained samples were cylindrical with a diameter of 15.3 mm and a height of 4–6 mm. SPS temperature was measured using an optical pyrometer IR-AHS (Hitachi, Japan) focused at the hole (5.5 mm deep) in the middle of the outer die wall. Graphite foil 0.2 mm thick was employed to prevent contact between the die and sintered material. Final samples were cylindrically shaped with an outer diameter of 10.3 mm and a height of 4–5 mm.

2.5. Characterization methods

Particle size distribution was determined on a particle size analyzer Analysette-22 NanoTec/MicroTec/XT Fritsch (Germany). Scanning electron microscopy (SEM) was performed on a CrossBeam 1540 XB Carl Zeiss (Germany) equipped with the add-on for energy-dispersive X-ray spectral analysis (EDX) Bruker (Germany). XRD was carried out on a D8 Advance Bruker AXS (Germany) diffractometer. Vickers microhardness was determined at 0.2 N load on a microhardness tester HMV-G-FA-D Shimadzu (Japan). The IR absorption spectra of the samples were recorded in the range of 400–4000 cm^{-1} using a Spectrum-1000 Fourier transform spectrometer PerkinElmer (USA). The thermogravimetric curves were recorded on the DTG-60H Shimadzu device in platinum crucibles with a pierced lid in a dry argon stream (20 mL/min) in the temperature range of 35–1300 °C and the heating rate of 10 °C/min. The weight of the attachments was about 40 mg, weighing was carried out on Sartorius CP2P micro weights with an accuracy of 1 μg.

Compressive strength ($\sigma_{cs.}$) was evaluated on a tensile machine Autograph AG-X plus 100 kN Shimadzu (Japan). Experimental density was measured by hydrostatic weighing on the balance Adventurer OHAUS Corporation (USA). Appearance density was found as a ratio of the experimental density (ED) measured via hydrostatic weighing to the theoretical density.

2.6. Evaluation of hydrolytic stability of (K, Cs)AlSi₃O₈ matrices

Dissolution stability of matrices was estimated based on leaching rate of cesium under long-term contact (30 days) with the distilled water (pH 6.8) at room temperature (25°C) in static condition. The well-known Russian Government Standard (GOST R 52126–2003), closely related to the ANSI/ANS-American National Standards Institute/American Nuclear Society 2019 (ANSI/ANS 16.1). Cesium, aluminum, potassium concentration was measured on an atomic absorption spectrometer SOLAAR M6 Thermo Scientific (USA).

The calculation of the effective diffusion coefficient (D_e) was performed by mathematical transformations of the second Fick law according to the method described in the paper [28]:

$$\frac{\sum m}{M_0} = 2 \left(\frac{D_e}{\pi}\right)^{\frac{1}{2}} \left(\frac{S}{V}\right) t^{\frac{1}{2}} + \alpha \tag{1}$$

where is m – cesium weight, mg, leaching time t, s, M_0 – initial cesium content in the sample, mg, D_e – effective diffusion coefficient, cm^2/s, S – the surface area of the sample, cm^2, V – a volume of sample, cm^3, α – parameter that takes into account the initial leaching of cesium, not related to diffusion (cesium leaches out at the initial contact of the leaching solution with the sample surface).

To calculate this equation was reduced to a linear form by introducing the coefficient K, which is the tangent of the slope angle of the direct dependence of the cesium fraction leached from the sample on the square root of the contact time of the material with the leaching agent:

$$K = 2 \left(\frac{D_e}{\pi}\right)^{0.5} \cdot \left(\frac{S}{V}\right) \tag{2}$$

The effective diffusion coefficient was calculated according to Eq. (3):

$$D_e = \frac{K^2 \cdot \pi}{4} \cdot \left(\frac{V}{S}\right)^2 \tag{3}$$

The leaching index (L) was calculated as the decimal logarithm of the inverse diffusion value [29].

$$L = \lg \frac{1}{D_e} \tag{4}$$

Evaluation of the dominant leaching mechanism based on the dependence of the decimal logarithm of the accumulated fraction of leached radionuclide (B_t, mg/m^2) on the decimal logarithm of the leaching time t, s:

$$\lg (B_t) = \frac{1}{2}\lg t + \lg \left[U_{max}d\sqrt{\frac{D_e}{\pi}}\right] \tag{5}$$

where is U_{max} – the maximum amount of leached radionuclide, mg/kg, d – matrix density, kg/m^3.

The leaching depth of the matrix characterizes the destruction of the matrix as a whole when it is in an aqueous medium. Eq. 8 calculated this characteristic:

$$L_t^i = \sum_1^n \left(W_n^i \cdot \frac{t_n}{d}\right) \tag{6}$$

where is L_t^i – the leaching depth of the matrix reached during the time interval t_n, cm, d – density of the sample, g/cm^3.

3. Results and discussions

3.1. Characterization of KAlSi₃O₈ and solid-state matrices

The character of the XRD curve with a blurred maximum in the angle range of 15–35° of the synthesized sample corresponded to an amorphous substance (Fig. 2a).

According to sorption isotherm (Fig. 2c), the maximum adsorption capacity A_{max} of amorphous KAlSi₃O₈ under static conditions towards Cs$^+$ ions from an aqueous solution at 20 °C and the ratio S:L of 1:40 after 3 h reached ~ 3.7 mmol/g. The maximum sorption capacity was achieved at an equilibrium concentration of Cs$^+$ ~15 mmol/L (Fig. 2c). The sorption isotherm belonged to the C-type according to the Giles classification, which was characterized by a linear increase in the sorption capacity with an increase in the equilibrium concentration. This type of isotherms is characteristic of the homogeneity of the adsorption centers of the material, characterized by an average affinity for the adsorbate.

The studied sample after saturation with cesium ions was amorphous (Fig. 2a). The results of the thermogravimetric study of the initial KAlSi₃O₈ and the cesium-saturated sample is shown in Fig. 2b. When the temperature increase, firstly physically adsorbed water was monotonously removed, then the decomposition of crystallohydrates and dehydration of aluminum hydroxide was observed. The removal of the main mass of water occurred at 600 – 1000°C with a total weight loss of 20.7% and 15.9% for KAlSi₃O₈ and cesium-saturated samples.

Fig. 2d shows the IR spectrum of the KAlSi₃O₈ and (Cs, K)AlSi₃O₈ powders. For both samples, an intense absorption band in the region of 850–1100 cm^{-1} was recorded, associated with valence Si–O–Si and Al–O–Al bonds vibrations. Importantly, that in the sample saturated with cesium, compared with the initial aluminosilicate, there was a slight shift of this absorption band to the region of lower frequencies. It was associated with the partial destruction of the aluminosilicate framework structure. Low-frequency absorption bands in the region of
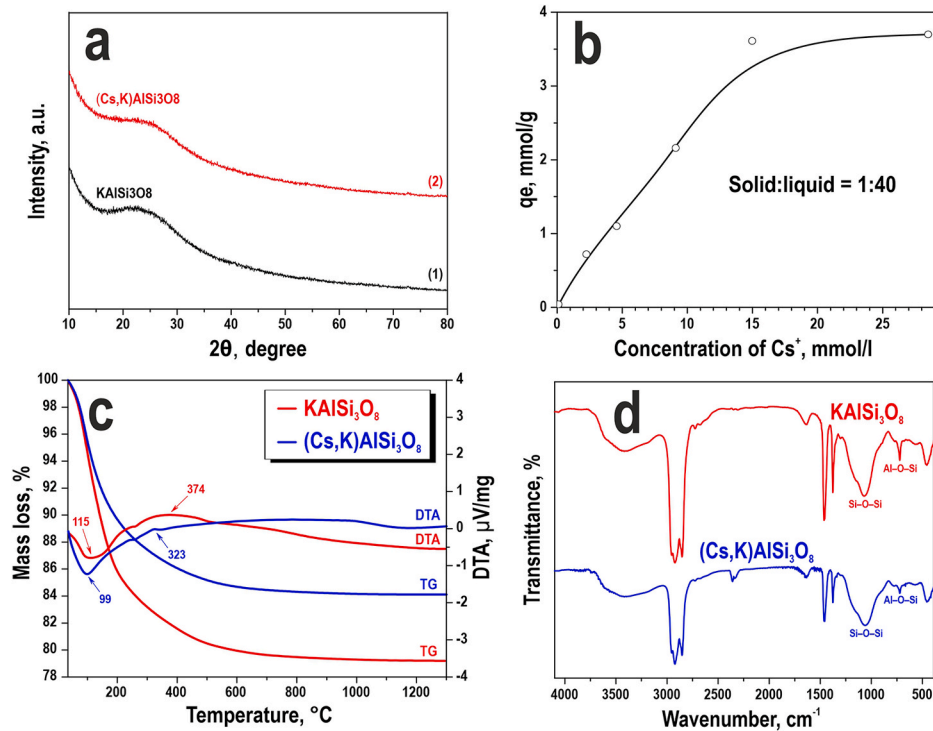
Fig. 2. Characteristics of the initial powder $KAlSi_3O_8$: a – XRD patterns; b – sorption isotherm of Cs^+ ions; c – thermogravimetric analysis; d – FT-IR spectra of $KAlSi_3O_8$ and $(Cs, K)AlSi_3O_8$.

450–600 cm^{-1} were characteristic of Si–O–Si and Al–O–Si deformation bonds vibrations. Deformation and valence O–H vibrations of the crystallization water caused the absorption bands in the region of 1600 and 3100-3650 cm^{-1}, respectively. The maximum of the absorption band of the valence water vibrations 3450 cm^{-1} was slightly lower for the valence O–H vibrations of free water (~3600 cm^{-1}). It was due to the

presence of water hydrogen bonds with the aluminosilicate crystal lattice and a potassium cation [30].

The low-temperature nitrogen adsorption-desorption of pristine $KAlSi_3O_8$ samples and after their saturation with cesium ions (Cs, K) $AlSi_3O_8$ was carried out. The isotherms for all samples had a capillary-condensation hysteresis loop and belong to type IV according to the
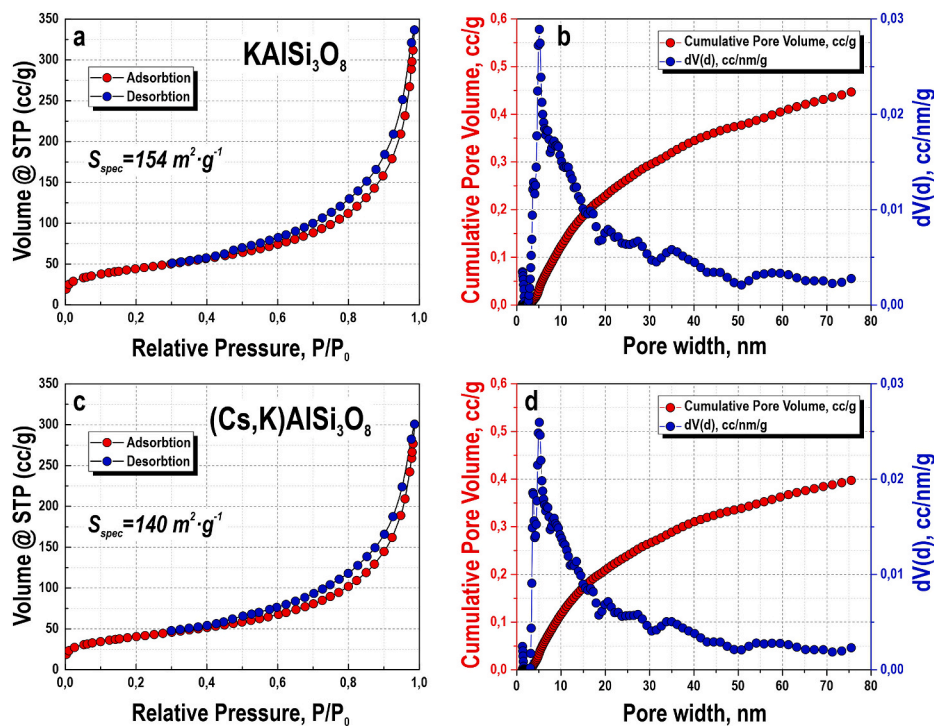
Fig. 3. Isotherm of low-temperature nitrogen adsorption-desorption (a,c) and DFT pore size distributions (b, d) of $KAlSi_3O_8$ powder before and after Cs^+ sorption saturation.

IUPAC classification [31,32], which is characteristic for mesoporous materials. Adsorbents had a set of micro-, meso- and macropores, with a certain predominance of 2–45 nm mesopores (Fig. 3a, b). It was confirmed by the isotherm treatment by the DFT method (Fig. 3b, d). The specific surface area (A_{BET}) for $KAlSi_3O_8$ and (Cs, K) $AlSi_3O_8$ samples was 154 and 140 m^2/g, respectively. A non-significant decrease in the specific surface after saturation with Cs^+ ions was observed due to the effect of K^+ ion exchange on Cs^+, which led to changes in the composite textural characteristics. The hysteresis loop for pristine and spent adsorbents had H3 type form. It means that the lower limit of the desorption branch is normally located at the cavitation-induced p/p_0. Loops of H3 type are given by non-rigid aggregates of plate-like particles (e.g., certain clays) but also if the pore network consists of macropores which are not completely filled with pore condensate.

The preparation of solid-state matrices using the SPS technology was carried out using the obtained (Cs, K)$AlSi_3O_8$ powder, containing Cs^+ ions ~23.3 wt%. The provided concentration of Cs^+ ions in alumino-silicate matrices is adequate, due to futures of their crystalline structure and possibility to chemical bounding of ^{137}Cs radionuclides. The provided results for containing of Cs^+ in nanostructured $KAlSi_3O_8$ spent adsorbent was supported by complex of physical-chemical techniques [33]. It was justified by atomic AAS, ICP-AES, ICP-MS analyses of aqueous solution obtained by dissolution of saturated adsorbent with 0.1 M $CsNO_3$ and by results of EDX analysis of spent adsorbent. The adsorbent dissolution was performed use of HF and HNO_3 acids mixture.

In addition, it should be noted that mineral-like materials with pollucite structure $Cs_4NaAl_5Si_{11}O_{32} \cdot 1,3H_2O$ can immobilize up to 42 wt% Cs^+ ions [34]. The synthetic pollucite has a chemical composition with stoichiometric formula $CsAlSi_2O_6$ [35], low coefficient of thermal expansion and thermal stability up to 1000°C. The releasing of cesium ions in aqueous solution reaches high values of up to $2 \cdot 10^{-8}$ $g/cm^2 \cdot day$ [19,36,37].

The granulometric sample composition of $KAlSi_3O_8$ was represented by a wide fraction of particles with a size of 0.5–100 μm (Fig. 4a). The smallest fraction was less than 1 μm (Area A1). The average fraction was 5–50 μm in the form of agglomerates of smaller particles (Area A1) and the large (main) fraction was represented by particles with a size of 50 to 100 μm (Area A3). It was also confirmed by the SEM data (Fig. 4b-d). As well as, the particle size distribution (PSD) and SEM analyses of (Cs, K) $AlSi_2O_8$ sample after saturation with Cs^+ ions were performed. The obtained results showed the absence of differences in particle size of $KAlSi_2O_8$ and (Cs, K)$AlSi_2O_8$ samples (Fig. 4b).

It was determined that sintering proceeded in two stages according to the dilatometric measurments (Fig. 5a). Stage I occurred at the process beginning during the first minutes of synthesis (up to 2 min) and was caused by particles rearrangement and packing under mechanical
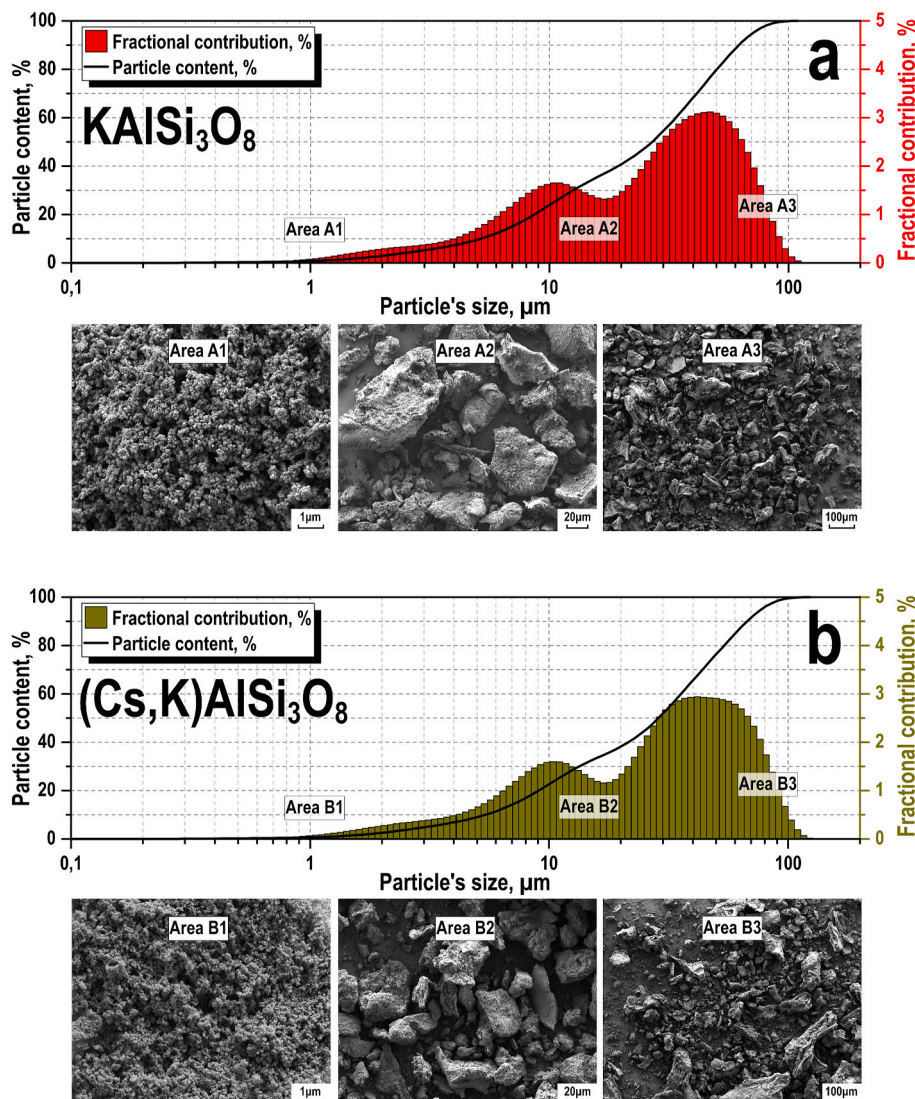
Fig. 4. Particle size distribution and SEM images of (a) $KAlSi_3O_8$ and (b) (Cs, K)$AlSi_3O_8$ powder samples.
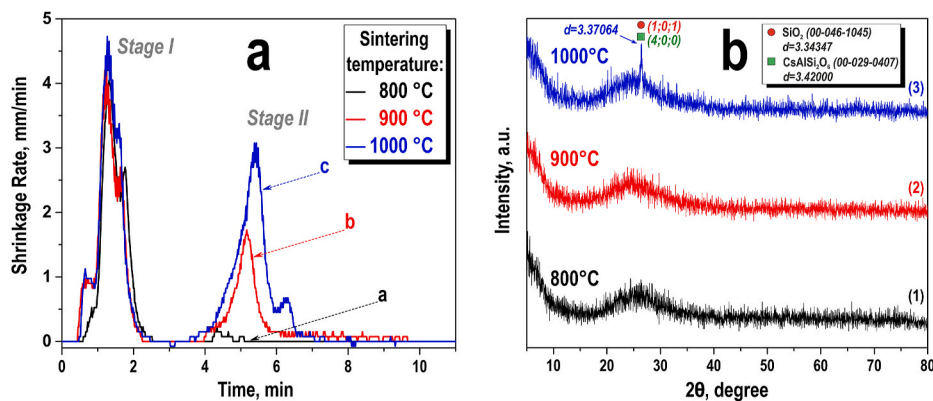
Fig. 5. The dilatometric curves (a) of (Cs, K)AlSi$_3$O$_8$ powder and XRD patterns (b) of solid-state matrices obtained by SPS at various temperatures.

action during powder pressing. The shrinkage rate at this stage was 4.5 mm/min, regardless of the sintering temperature. Stage II included thermal action on the powder along with the applied pressing. This process was the main sintering stage, since during heating, the processes of diffusion, plastic deformation, and viscous flow of the material were

activated. Primarily in the area of particle contact, which intensified the shrinkage of the sintered powder. (Cs, K)AlSi$_3$O$_8$ powder sintering did not occur at a temperature of 800 °C, since there was no shrinkage at this stage (Fig. 5a, curve 1). The sintering process was observed at 900 and 1000 °C, which was due to active powder shrinkage at a rate of 1.5 and 3
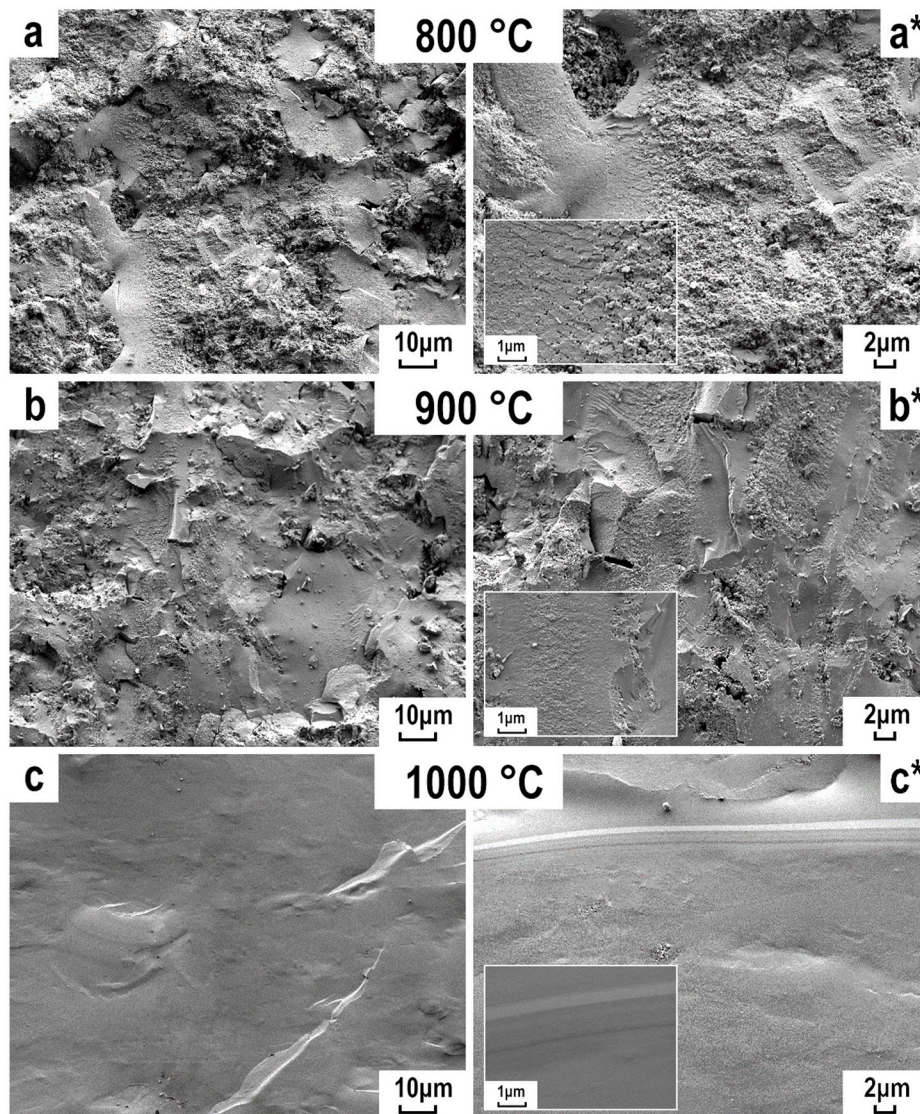
Fig. 6. SEM images of (Cs, K)AlSi$_3$O$_8$ solid matrices obtained by SPS at various temperatures.

mm/min, respectively. The shrinkage time was no more than 2 min (Fig. 5a, curves 2 and 3).

According to the XRD data (Fig. 5b), the amorphous (Cs, K)AlSi$_3$O$_8$ sample did not crystallize at 800–900 °C. In the composition of the sample obtained at 1000 °C, the formation of an insignificant impurity of the crystalline pollucite phase was observed (Fig. 5b, curve 3). When the temperature rose above 1000 °C, the aluminosilicate passed into the liquid melt. The main mechanism of Cs$^+$ ions adsorption was ion-exchange process. According to XRD data (Fig. 5b, curve 3). there is too weak peak at 2 theta ~26°, which can belong to SiO$_2$ (quartz, 00-046-1045) and CsAlSi$_2$O$_6$ (pollucite, 00-029-0407). The presence of this compounds could be due to crystallization processes in aluminosilicate matrices during SPS sintering. But very weak intensity of this peak do not allow to make clear conclusion. The proposed discussion was supported by EDX elements mapping on the sample surface (Fig. 7, sample obtained at 1000 °C). Therefore, it was shown that Cs, K, Al, and Si had homogenous distribution in the same surface field. However, there is field with high Si concentration and absence of Cs, K, Al atoms. So, there are two type of surface sample with different contents of Cs, K, Al, and Si elements. In that case, it could be due to presence of two crystalline phases of SiO$_2$ (quartz) and CsAlSi$_2$O$_6$ (pollucite).

The consolidated samples structure varied depending on the process temperature (Fig. 6). SEM image of the sample obtained at 800 °C showed that the sintering processes were only initiated. Both sintered areas in the form of monolithic inclusions and loose areas in the form of compressed and partially sintered particles of the initial powder were presented (Fig. 6a, a*). When the temperature increased up to 900 °C, the area of monolithic agglomerates expended significantly due to the intensification of sintering processes. Meanwhile, the presence of an insignificant number of micro defects in the sample volume was detected (Fig. 6b, b*). When the temperature reached 1000 °C, the aluminosilicate sample had a monolithic, non-porous and defect-free structure (Fig. 6c, c*).

According to the EDX analysis data (Fig. 7), the distribution of the main elements over the matrices surface could be considered uniform, in particular, cesium was integrated throughout the entire volume of the samples.

The physical and mechanical characteristics of the (Cs, K)AlSi$_3$O$_8$ matrices were directly proportional to the temperature of SPS performing. The density, compressive strength, and Vickers microhardness increased with a rise in the sintering temperature (Fig. 8). These parameters increased sharply at the sintering temperature from 900 °C and above, which indicated the efficiency of (Cs, K)AlSi$_3$O$_8$ powder sintering under these conditions. It was consistent with the previously noted powder shrinkage rate (Fig. 5a).

An increase in the dispersion and asymmetry of the distribution of microhardness values relative to the statistical median line in the box and Vickers diagram indicated an increase in the structural heterogeneity of the (Cs, K)AlSi$_3$O$_8$ samples. It was observed during increase in the SPS temperature (Fig. 8). The range of microhardness values in the statistical sample was due to the anisotropy of the properties formed because of partial crystallization, which was previously confirmed by XRD data (Fig. 5b).

3.2. Cesium leaching study

The dissolution stability of the (Cs, K)AlSi$_3$O$_8$ matrices was evaluated, which was the main indicator of their effectiveness for the cesium radionuclide immobilization. The lowest rate of cesium leaching was observed for the sample obtained at 1000 °C (Fig. 9a). This parameter reached $6.94 \cdot 10^{-7}$ g cm^{-2}·day^{-1}, which met the GOST R 50926-96 requirements for solidified high-level waste. It was obvious that the high hydrolytic stability of the samples was due to their glass-like structure. The increase in this parameter for samples obtained at an elevated sintering temperature was due to the formation of the pollucite phase in their composition (Fig. 5b). It is known that the pollucite form of aluminosilicate, both a natural mineral and its synthetic form, is capable of providing high chemical binding of cesium ions up to 42 wt% [26,38].

The value of the tangent of the angle of inclination of the straight lines (Fig. 9b) was close to 0.5, which indicated the predominance of the diffusion leaching mechanism, according to the Groot and Van der Sloot model [39,40]. (Cs, K)AlSi$_3$O$_8$ matrices were characterized by a low cesium diffusion coefficient (De), due to strong chemical cesium bounding and low number of defects and open pores in the obtained matrices structure (Table 1).

The leaching index (L) of all samples was higher than 8, which allowed concluding that cesium was reliably fixed in the volume of the material and that the synthesized matrices can be used as immobilizing materials [41]. The calculated parameters of the leaching depth were shown in Fig. 9c. Solid-state aluminosilicate samples had great stability in an aqueous environment due to the dense structure and chemical resistance of obtained matrices.

3.3. Comparison study

A comparative analysis of the qualitative characteristics of the (Cs, K)AlSi$_3$O$_8$ matrices obtained at 1000 °C and the regulatory document requirements for solidified radioactive waste, showed that the developed solid-state aluminosilicate had high-quality characteristics and comply with the regulatory requirements (Table 2)
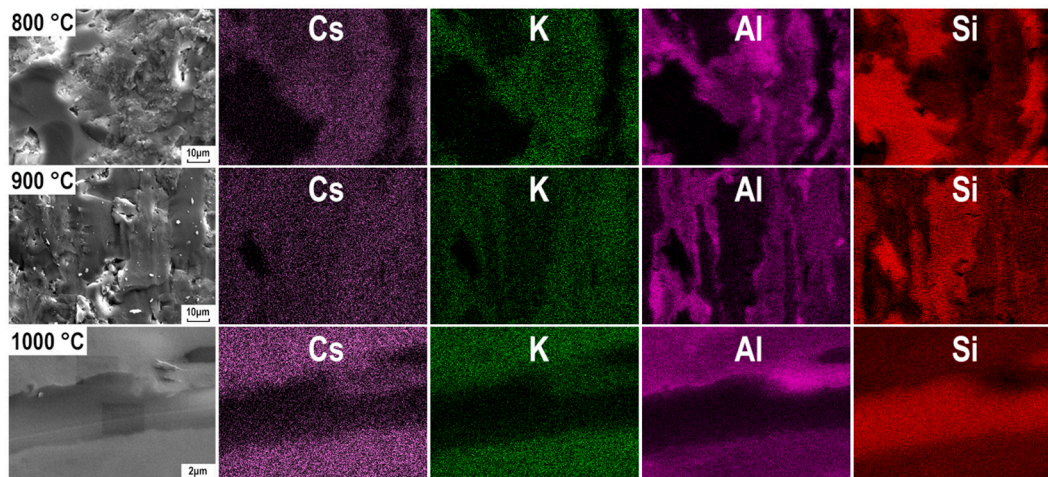
Fig. 7. EDX element mapping of (Cs, K)AlSi$_3$O$_8$ solid matrices obtained by SPS at various temperatures.
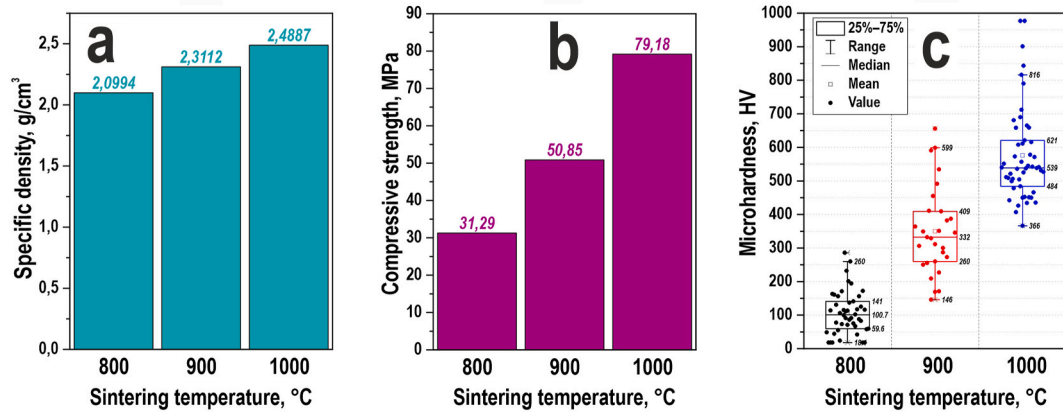
Fig. 8. Physical-mechanical characteristics of $(Cs,K)AlSi_3O_8$ solid matrices obtained by SPS at various temperatures: a – appearance density; b – compressive strength; c – diagrams of Vickers microhardness.
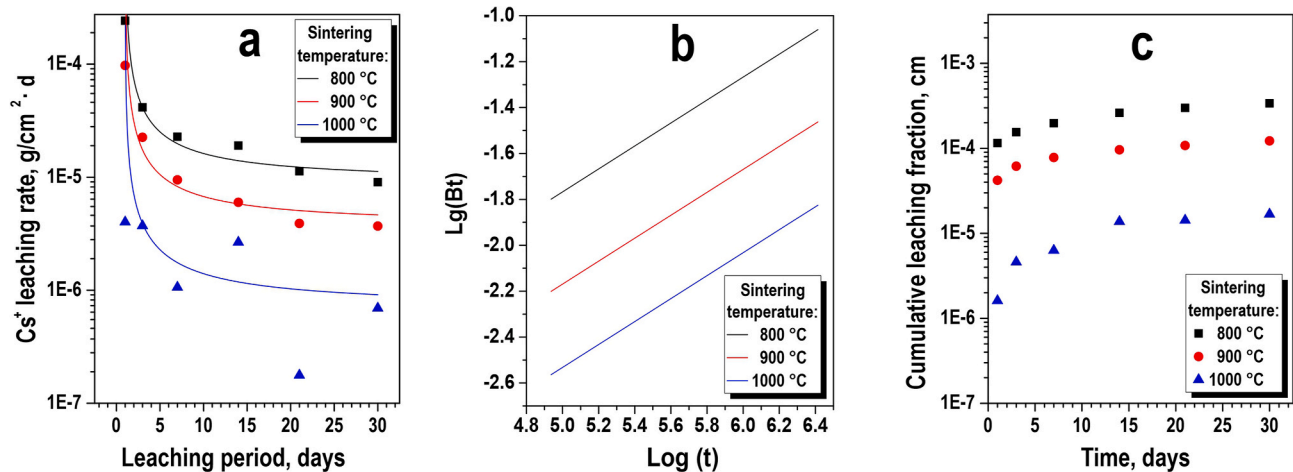
Fig. 9. Dissolution stability of $(Cs, K)AlSi_3O_8$, matrices obtained by SPS at various temperatures: a – rate of cesium leaching; b – logarithmic dependences of the accumulated fraction of leached cesium on the leaching time from the samples; c – depth of penetration of the leaching agent into the matrix L_t.

Table 1
Cesium leaching parameters for $(Cs, K)AlSi_3O_8$ matrices obtained by SPS at various temperatures.

Sintering temperature, °C	D_e, cm²/s	L	U max, mg/kg
800	$2.16 \cdot 10^{-9}$	8.66	$3.28 \cdot 10^{-2}$
900	$3.84 \cdot 10^{-9}$	8.41	$7.36 \cdot 10^{-2}$
1000	$7.36 \cdot 10^{-9}$	8.13	$7.71 \cdot 10^{-3}$

Note: values error of ±5%.

It was established that the SPS technology is more technologically attractive compared to traditional sintering methods. The results of Table 3 are clear supported the advantages of developed cesium-saturated matrices in comparison with analogs materials. The temperature conditions for matrices obtained by the SPS technique were lower, as well as the heating and holding cycle time was minimal. The main qualitative characteristics of the studied matrices in most cases exceeded the required parameters and described analogs (Table 3).

4. Conclusion

An amorphous $KAlSi_3O_8$ aluminosilicate with a high sorption capacity towards cesium ions of ~3.7 mmol/g was synthesized by precipitation from an alkaline silica solution. Solid-state matrices of amorphous composition based on synthesized $(Cs, K)AlSi_3O_8$ powder

Table 2
Quality characteristics for solid radioactive wastes and obtained aluminosilicate matrices.

Parameter	Requirements of GOST R 50926-96	The sample obtained by SPS at 1000°C	Testing method
Chemical stability (leaching rate): ^{133}Cs, g/cm²·day	No more 10^{-5}	$6.94 \cdot 10^{-7}$	GOST R 52126-2003 (ISO 6961:1982)
Compressive strength, MPa	No less 9	79	Tests on a bursting machine
Thermal stability (no changes in the structure and chemical composition at temperature), °C	No less 550	Up to 1000	XRD and SEM
Homogeneity of the glass block structure in the volume	Homogeneous	Tests on a bursting machine	XRD and SEM

were obtained using the SPS technique. Thermal stability of pristine aluminosilicate and cesium-saturated form $(Cs, K)AlSi_3O_8$ during heat treatment in an inert medium up to 1200 °C was shown. The obtained matrices with a uniform cesium distribution by volume had high values of relative density (up to 99.9%), compressive strength (31.3 – 79.2

Table 3
Comparative characteristics of solid-state matrices for cesium immobilization.

Type of matrices [Ref.]	Sintering method	Heating rate, °C·min^{-1};	Sintering atmosphere	Exposure time, h	Sintering temperature, °C	Cesium leaching rate, g·m^{-2}·day^{-1}
$Ba_{0.8}Cs_{0.4}Al_2Ti_6O_{16}$ [42]	cold pressing followed by sintering	10	air	5	1300	7.83×10^{-3}
$3CaO \cdot Al_2O_3 \cdot 3CaSO_4 \cdot 32H_2O$ [43]	cold pressing followed by sintering	5	air	2	1310	6.21×10^{-3}
SAP $(SiO_2 \cdot Al_2O_3 \cdot P_2O_5)$ [44]	sintering without pressure	–	air	4	1150	$10^{-2} \sim 10^{-3}$
$Cs_3(PMo_{12}O_{40}) + Cs_4Al_4Si_{20}O_{48}$ [45]	cold pressing followed by sintering	–	–	1	1200	4.7×10^{-2} 3.9×10^{-4}
$K_{1-x}Cs_xAlSi_2O_6$ [46]	sintering without pressure	10	air	2	1300	$4.35 \times 10^{-2} - 8 \times 10^{-4}$
Natural mordenite powder (Iizaka mine, Nitto Funka Co) [47]	sintering without pressure	10	air	1	1100	Not provided
Shabazite (general composition: $K_2Al_2Si_4O_{12}$) with Cs^+ [48]	sintering without pressure	10	air	1	1100	Not provided
$Ba_{1-x}(La, Cs)_xZrO_3$ [49]	sintering without pressure	–	air	2	900	0.9×10^{-3}
$Cs_2O \cdot Al_2O_3 \cdot 4.3SiO_2/Cs_2O \cdot Al_2O_3 \cdot 4.3SiO_2 \cdot B_2O_3$ [21]	sintering without pressure	–	air	3	1200/950	Not provided
raw material to prepare (0.3Na, 0.7Cs)-geopolymer ((0.3Na,0.7Cs)-GP)+B_2O_3 [29]	sintering without pressure	5	argon	2	600–1000	10^{-4}
Synthesis of pollucite from (0.3X, 0.7Cs)-based geopolymer and their doping-enhanced immobilization performance of Cs (X = Li, Na and K)) [50]	sintering without pressure	5	air	2	≤1000	$2,51 \times 10^{-4}$
Cs–NZP [51]	Microwave	–	air	3	1000	$1.5 \times 10^{-3} - 1.2 \times 10^{-5}$
Na-A (Cs – LTA) [18]	hot pressing	10	argon	3	750	9.3×10^{-2}
Natural zeolite from the Far Eastern deposit (Russia) [26,52]	SPS	100	vacuum	0.08	1000	$10^{-3} - 10^{-5}$
$Cs_{0.9}Ca_{0.5}K_{1.1}[Al_3Si_8O_{22}]$ [53]	SPS	50	vacuum	0.16	1100	$1.13 \pm 0.12 \times 10^{-3}$
$(Cs_{0.15}(3)K_{0.57}(4)Al_{0.90}(4)Si_{2.24}(5)O_6)$ [54]	hot pressing	–	argon	4	1050–1250	Not provided
$CsAlSi_5O_{12}$ [55]	hot pressing	–	–	3	950	low Cs leaching rate

MPa), and Vickers microhardness (0.9–5.3 GPa). The highest dissolution stability was possessed by a high-temperature samples obtained at 1000 °C, where the cesium leaching rate (R_{Cs}) did not exceed 10^{-7} g cm^{-2}·day^{-1} and the diffusion coefficient (D_e) was 7.36×10^{-9} cm^2/s. The high quality of the obtained products was confirmed by compliance with GOST R 50926-96 and characteristics of described analogs. The developed aluminosilicate matrices are of practical interest for the purification technologies and radioactive waste processing, and the creation of radioisotope products.

Declaration of competing interest

The authors declare that they have no known competing financial interests or personal relationships that could have appeared to influence the work reported in this paper.

Acknowledgments

References

[1] D. Alby, C. Charnay, M. Heran, B. Prelot, J. Zajac, Recent developments in nanostructured inorganic materials for sorption of cesium and strontium: synthesis and shaping, sorption capacity, mechanisms, and selectivity—a review, J. Hazard Mater. 344 (2018) 511–530, https://doi.org/10.1016/j.jhazmat.2017.10.047.

[2] Ö. Arar, Application of sorption process for the removal of radioactive elements, in: A. Núñez-Delgado (Ed.), Sorbents Mater. Control. Environ. Pollut., Elsevier, 2021, pp. 495–512, https://doi.org/10.1016/B978-0-12-820042-1.00020-1.

[3] V.A. Avramenko, A.M. Egorin, E.K. Papynov, T.A. Sokol'nitskaya, I.G. Tananaev, V. I. Sergienko, Processes for treatment of liquid radioactive waste containing seawater, Radiochemistry 59 (2017), https://doi.org/10.1134/S1066362217040142.

[4] A.I. Orlova, M.I. Ojovan, Ceramic mineral waste-forms for nuclear waste immobilization, Materials (Basel) 12 (2019) 2638, https://doi.org/10.3390/ma12162638.

[5] B.L. Phoon, C.W. Lai, J.C. Juan, P.L. Show, W.H. Chen, A review of synthesis and morphology of SrTiO3 for energy and other applications, Int. J. Energy Res. 43 (2019) 5151–5174, https://doi.org/10.1002/er.4505.

[6] S. Yu, H. Mei, X. Chen, X. Tan, B. Ahmad, A. Alsaedi, T. Hayat, X. Wang, Impact of environmental conditions on the sorption behavior of radionuclide 90Sr(II) on Na-montmorillonite, J. Mol. Liq. 203 (2015) 39–46, https://doi.org/10.1016/j.molliq.2014.12.041.

[7] C.B. Durrant, J.D. Begg, A.B. Kersting, M. Zavarin, Cesium sorption reversibility and kinetics on illite, montmorillonite, and kaolinite, Sci. Total Environ. 610–611 (2018) 511–520, https://doi.org/10.1016/j.scitotenv.2017.08.122.

[8] C. Joseph, J. Mibus, P. Trepte, C. Müller, V. Brendler, D.M. Park, Y. Jiao, A. B. Kersting, M. Zavarin, Long-term diffusion of U(VI) in bentonite: dependence on density, Sci. Total Environ. 575 (2017) 207–218, https://doi.org/10.1016/j.scitotenv.2016.10.005.

[9] W. Baek, S. Ha, S. Hong, S. Kim, Y. Kim, Cation exchange of cesium and cation selectivity of natural zeolites: chabazite, stilbite, and heulandite, Microporous Mesoporous Mater. 264 (2018) 159–166, https://doi.org/10.1016/j.micromeso.2018.01.025.

[10] W.C. Jolin, M. Kaminski, Sorbent materials for rapid remediation of wash water during radiological event relief, Chemosphere 162 (2019) 165–171, https://doi.org/10.1016/j.chemosphere.2016.07.077.Sorbent.

[11] J. Neumann, H. Brinkmann, S. Britz, J. Lützenkirchen, F. Bok, M. Stockmann, V. Brendler, T. Stumpf, M. Schmidt, A comprehensive study of the sorption

mechanism and thermodynamics of f-element sorption onto K-feldspar, J. Colloid Interface Sci. 591 (2021) 490–499, https://doi.org/10.1016/j.jcis.2020.11.041.

[12] M. Jiménez-Reyes, P.T. Almazán-Sánchez, M. Solache-Ríos, Radioactive waste treatments by using zeolites. A short review, J. Environ. Radioact. 233 (2021), https://doi.org/10.1016/j.jenvrad.2021.106610.

[13] B.K. Singh, R. Tomar, R. Tomar, S.S. Tomar, Sorption of homologues of radionuclides by synthetic ion exchanger, Microporous Mesoporous Mater. 142 (2011) 629–640, https://doi.org/10.1016/j.micromeso.2011.01.006.

[14] B.K. Singh, R. Tomar, S. Kumar, A. Jain, B.S. Tomar, V.K. Manchanda, Sorption of 137Cs, 133Ba and 154Eu by synthesized sodium aluminosilicate (Na-AS), J. Hazard Mater. 178 (2010) 771–776, https://doi.org/10.1016/j.jhazmat.2010.02.007.

[15] D. Alby, C. Charnay, M. Heran, B. Prelot, J. Zajac, Recent developments in nanostructured inorganic materials for sorption of cesium and strontium: synthesis and shaping, sorption capacity, mechanisms, and selectivity—a review, J. Hazard Mater. 344 (2018) 511–530, https://doi.org/10.1016/j.jhazmat.2017.10.047.

[16] A. Khaleque, M.M. Alam, M. Hoque, S. Mondal, J. Bin Haider, B. Xu, M.A.H. Johir, A.K. Karmakar, J.L. Zhou, M.B. Ahmed, M.A. Moni, Zeolite synthesis from low-cost materials and environmental applications: a review, Environ. Adv. 2 (2020) 100019, https://doi.org/10.1016/j.envadv.2020.100019.

[17] C.M. Jantzen, M.I. Ojovan, On selection of matrix (wasteform) material for higher activity, Nuclear Waste Immobilization (Review) 64 (2019) 1611–1624, https://doi.org/10.1134/S0036023619130047.

[18] M. Omerašević, L. Matović, J. Ružić, Ž. Golubović, U. Jovanović, S. Mentus, V. Dondur, Safe trapping of cesium into pollucite structure by hot-pressing method, J. Nucl. Mater. 474 (2016) 35–44, https://doi.org/10.1016/j.jnucmat.2016.03.006.

[19] T.A. Vereshchagina, S.N. Vereshchagin, N.N. Shishkina, N.G. Vasilieva, L.A. Solovyov, A.G. Anshits, Microsphere zeolite materials derived from coal fly ash cenospheres as precursors to mineral-like aluminosilicate hosts for 135,137Cs and 90Sr, J. Nucl. Mater. 437 (2013) 11–18, https://doi.org/10.1016/j.jnucmat.2013.01.343.

[20] J. Luo, X. Li, F. Zhang, S. Chen, D. Ren, Sintering of monoclinic-SrAl2Si2O8 ceramics and their immobilization of Sr, Int. J. Miner. Metall. Mater. (2020), https://doi.org/10.1007/s12613-020-2056-6 ©.

[21] S. Chen, J.F. Guo, B. Xu, X.W. Sun, Sintering of Metakaolin-based Na-Pollucite ceramics and their immobilization of Cs, Ann. Nucl. Energy 145 (2020), https://doi.org/10.1016/j.anucene.2020.107595.

[22] L.D. Gardner, M.S. Wasnik, B.J. Riley, S. Chong, M.F. Simpson, K.L. Carlson, Synthesis and characterization of sintered H–Y zeolite-derived waste forms for dehalogenated electrorefiner salt, Ceram. Int. 46 (2020) 17707–17716, https://doi.org/10.1016/j.ceramint.2020.04.075.

[23] E.K. Papynov, Spark plasma sintering of ceramic and glass-ceramic matrices for cesium radionuclides immobilization, in: K. Narang (Ed.), Glas. Prop. Appl. Technol., Nova Science Publishers, Inc., New York, 2018, pp. 107–153.

[24] E.K. Papynov, O.O. Shichalin, V.Y. Mayorov, E.B. Modin, A.S. Portnyagin, I.A. Tkachenko, A.A. Belov, E.A. Gridasova, I.G. Tananaev, V.A. Avramenko, Spark Plasma Sintering as a high-tech approach in a new generation of synthesis of nanostructured functional ceramics, Nanotechnologies Russ 12 (2017) 49–61, https://doi.org/10.1134/S1995078017010086.

[25] E.K. Papynov, A.A. Belov, O.O. Shichalin, I.Y. Buravlev, S.A. Azon, A.V. Golub, A.V. Gerasimenko, Y.A. Parotkina, A.P. Zavjalov, I.G. Tananaev, V.I. Sergienko, SrAl2Si2O8 ceramic matrices for 90Sr immobilization obtained via spark plasma sintering-reactive synthesis, Nucl. Eng. Technol. (2021) 2–7, https://doi.org/10.1016/j.net.2021.01.024.

[26] E.K. Papynov, O.O. Shichalin, V.Y. Mayorov, V.G. Kuryavyi, T.A. Kaidalova, L.V. Teplukhina, A.S. Portnyagin, A.B. Slobodyuk, A.A. Belov, I.G. Tananaev, V.A. Avramenko, V.I. Sergienko, SPS technique for ionizing radiation source fabrication based on dense cesium-containing core, J. Hazard Mater. 369 (2019) 25–30, https://doi.org/10.1016/j.jhazmat.2019.02.016.

[27] P.S. Gordienko, I.A. Shabalin, S.B. Yarusova, I.G. Zhevtun, S.B. Bulanova, Sorption of Cs+ ions from seawater by a nanostructured aluminosilicate sorbent, Inorg. Mater. 54 (2018) 1151–1156, https://doi.org/10.1134/S0020168518110079.

[28] P. Szajerski, A. Bogobowicz, A. Gasiorowski, Cesium retention and release from sulfur polymer concrete matrix under normal and accidental conditions, J. Hazard Mater. 381 (2020) 121180, https://doi.org/10.1016/j.jhazmat.2019.121180.

[29] P. He, S. Fu, M. Wang, X. Duan, Q. Wang, D. Li, Z. Yang, D. Jia, Y. Zhou, B2O3-assisted low-temperature crystallization of pollucite structures and their potential applications in Cs+ immobilization, J. Nucl. Mater. 540 (2020) 152314, https://doi.org/10.1016/j.jnucmat.2020.152314.

[30] S.B. Yarusova, P.S. Gordienko, A.E. Panasenko, N.N. Barinov, L.A. Zemnukhova, Sorption properties of sodium and potassium aluminosilicates from alkaline hydrolyzates of rice straw, Russ. J. Phys. Chem. A 93 (2019) 333–337, https://doi.org/10.1134/S003602441902033X.

[31] M. Thommes, K. Kaneko, A.V. Neimark, J.P. Olivier, F. Rodriguez-Reinoso, J. Rouquerol, K.S.W. Sing, Physisorption of gases, with special reference to the evaluation of surface area and pore size distribution (IUPAC Technical Report), Pure Appl. Chem. 87 (2015) 1051–1069, https://doi.org/10.1515/pac-2014-1117.

[32] E.K. Papynov, A.S. Portnyagin, E.B. Modin, V.Y. Mayorov, O.O. Shichalin, A.P. Golikov, V.S. Pechnikov, E.A. Gridasova, I.G. Tananaev, V.A. Avramenko, A complex approach to assessing porous structure of structured ceramics obtained by SPS technique, Mater. Char. 145 (2018) 294–302, https://doi.org/10.1016/j.matchar.2018.08.044.

[33] P.S. Gordienko, S.B. Yarusova, I.A. Shabalin, V.V. Zheleznov, N.V. Zarubina, S.B. Bulanova, Sorption properties of nanostructured potassium aluminosilicate, Radiochemistry 56 (2014) 607–613, https://doi.org/10.1134/S1066362214060058.

[34] L.H. Ortega, M.D. Kaminski, S.M. McDeavitt, Pollucite and feldspar formation in sintered bentonite for nuclear waste immobilization, Appl. Clay Sci. 50 (2010) 594–599, https://doi.org/10.1016/j.clay.2010.10.003.

[35] G.T. Kokotailo, Zeolite Crystallography. Zeolites: Science and Technology, Martinus Nijhoff Publishers, 1984.

[36] J. Balencie, D. Burger, J.L. Rehspringer, C. Estournès, S. Vilminot, M. Richard-Plouet, A. Boos, Perlite for permanent confinement of cesium, J. Nucl. Mater. 352 (2006) 196–201, https://doi.org/10.1016/j.jnucmat.2006.02.054.

[37] M. Luo, M. Wen, J. Wang, J. Zhu, The study of cooperation solidification of Cs based on ZSM-5 zeolite, Energy Procedia 39 (2013) 434–442, https://doi.org/10.1016/j.egypro.2013.07.234.

[38] E.K. Papynov, Spark plasma sintering of ceramic and glass-ceramic matrices for cesium radionuclides immobilization, in: K. Narag (Ed.), Glas. Prop. Appl. Technol., Nova Science Publisher, Inc, New York, 2018, pp. 109–153.

[39] D.S. Kosson, H.A. Van Der Sloot, T.T. Eighmy, An Approach for Estimation of Contaminant Release during Utilization and Disposal of Municipal Waste Combustion Residues, 1996, https://doi.org/10.1016/0304-3894(95)00109-3.

[40] G.J. de Groot, H.A. van der Sloot, Determination of Leaching Characteristics of Waste Materials Leading to Environmental Product Certification, ASTM Spec. Tech. Publ., 1992, https://doi.org/10.1520/stp19548s.

[41] R. Cioffi, M. Pansini, D. Caputo, C. Colella, Evaluation of mechanical and leaching properties of cement-based solidified materials encapsulating cd-exchanged natural zeolites, Environ. Technol. (United Kingdom) (1996), https://doi.org/10.1080/09593331708616491.

[42] J. Ma, Z. Fang, X. Yang, B. Wang, F. Luo, X. Zhao, X. Wang, Y. Yang, Investigating hollandite–perovskite composite ceramics as a potential waste form for immobilization of radioactive cesium and strontium, J. Mater. Sci. 56 (2021) 9644–9654, https://doi.org/10.1007/s10853-021-05886-2.

[43] X. Xu, H. Bi, Y. Yu, X. Fu, S. Wang, Y. Liu, P. Hou, X. Cheng, Low leaching characteristics and encapsulation mechanism of Cs+ and Sr2+ from SAC matrix with radioactive IER, J. Nucl. Mater. 544 (2021) 152701, https://doi.org/10.1016/j.jnucmat.2020.152701.

[44] K.R. Lee, B.J. Riley, H.S. Park, J.H. Choi, S.Y. Han, J.M. Hur, J.A. Peterson, Z. Zhu, D.K. Schreiber, K. Kruska, M.J. Olszta, Investigation of physical and chemical properties for upgraded SAP (SiO 2 –Al 2 O 3 –P 2 O 5) waste form to immobilize radioactive waste salt, J. Nucl. Mater. 515 (2019) 382–391, https://doi.org/10.1016/j.jnucmat.2019.01.004.

[45] Y. Wu, X.X. Zhang, Y.Z. Wei, H. Mimura, Development of adsorption and solidification process for decontamination of Cs-contaminated radioactive water in Fukushima through silica-based AMP hybrid adsorbent, Separ. Purif. Technol. 181 (2017) 76–84, https://doi.org/10.1016/j.seppur.2017.03.019.

[46] J. Li, J. Duan, L. Hou, Z. Lu, Effect of Cs content on K1-xCsxAlSi2O6 ceramic solidification forms, J. Nucl. Mater. 499 (2018) 144–154, https://doi.org/10.1016/j.jnucmat.2017.11.001.

[47] H. Aono, R. Takahashi, Y. Itagaki, E. Johan, N. Matsue, Cs immobilization using the formation of the glassy phase by the heat-treatment of natural mordenite, J. Nucl. Mater. 508 (2018) 20–25, https://doi.org/10.1016/j.jnucmat.2018.05.027.

[48] H. Aono, Y. Takeuchi, Y. Itagaki, E. Johan, Synthesis of chabazite and merlinoite for Cs+ adsorption and immobilization properties by heat-treatment, Solid State Sci. 100 (2020) 106094, https://doi.org/10.1016/j.solidstatesciences.2019.106094.

[49] J. Zhao, J. Li, H. Liu, X. Zhang, K. Zheng, H. Yu, Q. Lian, H. Wang, Y. Zhu, J. Huo, Cesium immobilization in perovskite-type Ba1-x(La, Cs)xZrO3 ceramics by sol-gel method, Ceram. Int. 46 (2020) 9968–9971, https://doi.org/10.1016/j.ceramint.2019.12.219.

[50] P. He, R. Wang, S. Fu, M. Wang, D. Cai, G. Ma, M. Wang, J. Yuan, Z. Yang, X. Duan, Y. Wang, D. Jia, Y. Zhou, Safe trapping of cesium into doping-enhanced pollucite structure by geopolymer precursor technique, J. Hazard Mater. 367 (2019) 577–588, https://doi.org/10.1016/j.jhazmat.2019.01.013.

[51] A.H. Microwave-assisted low temperature synthesis of sodium zirconium phosphate (NZP) and the leachability of some selected fission products incorporated in its structure - A case study of leachability of cesiumNaik, S.B. Deb, A.B. Chalke, M.K. Saxena, K.L. Ramakumar, V. Venugopal, S.R. Dharwadkar, Microwave-assisted low temperature synthesis of sodium zirconium phosphate (NZP) and the leachability of some selected fission products incorporated in its structure - a case study of leachability of cesium, J. Chem. Sci. 122 (2010) 71–82, https://doi.org/10.1007/s12039-010-0009-8.

[52] O.O. Shichalin, E.K. Papynov, V.Y. Maiorov, A.A. Belov, E.B. Modin, I.Y. Buravlev, Y.A. Azarova, A.V. Golub, E.A. Gridasova, A.E. Sukhorada, I.G. Tananaev, V.A. Avramenko, Spark plasma sintering of aluminosilicate ceramic matrices for immobilization of cesium radionuclides, Radiochemistry 61 (2019) 185–191, https://doi.org/10.1134/S1066362219020097.

[53] L.C. Harnett, L.J. Gardner, S.K. Sun, C. Mann, N.C. Hyatt, Reactive spark plasma sintering of Cs-exchanged chabazite: characterisation and durability assessment for Fukushima Daiichi NPP clean-up, J. Nucl. Sci. Technol. 56 (2019) 891–901, https://doi.org/10.1080/00223131.2019.1602484.

[54] L.J. Gardner, S.A. Walling, C.L. Corkhill, N.C. Hyatt, Thermal treatment of Cs-exchanged chabazite by hot isostatic pressing to support decommissioning of Fukushima Daiichi Nuclear Power Plant, J. Hazard Mater. 413 (2021) 125250, https://doi.org/10.1016/j.jhazmat.2021.125250.

[55] M. Omerašević, J. Ružić, B.N. Vasiljević, Z. Baščarević, D. Bučevac, J. Orlić, L. Matović, Transformation of Cs-exchanged clinoptilolite to CsAlSi5O12 by hot-pressing, Ceram. Int. 43 (2017) 13500–13504, https://doi.org/10.1016/j.ceramint.2017.07.055.